The 4th Joint International Conference on Multibody System Dynamics
May 29 – June 2, 2016, Montréal, Canada

Modeling and numerical simulation of anisotropic dry friction with non-convex friction force reservoir

Simon V. Walker[1] and Remco I. Leine[1]

[1] *Institute for Nonlinear Mechanics, University of Stuttgart, {walker,leine}@inm.uni-stuttgart.de*

ABSTRACT — *In this work an anisotropic dry friction model for non-convex friction force reservoirs is developed in the framework of convex analysis and implemented in a Moreau time-stepping scheme. Anisotropic friction occurs on a variety of technical surfaces. In order to accurately describe the constitutive behavior of stick and slip, set-valued force laws expressed as normal cone inclusions are formulated. Conventional normal cone inclusion force laws are limited to convex sets of admissible friction forces and are based on normality of the sliding direction on the force reservoir. We extend the existing model by allowing for non-convex star-shaped force reservoirs and ensuring normality of the sliding velocity on an independent arbitrary convex set. This highly general force law can be adjusted to measured anisotropic frictional behavior. The capability of the proposed normal cone inclusion force law to handle non-convex star-shaped force reservoirs in numerical simulations is shown. The set-valued force law accounts for stiction and enables the description of a large class of anisotropic dry friction models.*

1 Introduction

Anisotropic dry friction occurs in various technical applications. For example, machining or finishing of a surface can lead to an anisotropic surface roughness which in turn causes anisotropic frictional behavior. Anisotropy may also originate from the crystal structure of a material and occurs on the surface of composite, textile and biological materials [1]. On the one hand, it is often an unwanted side effect, which cannot be neglected. For instance in deep drawing of cold rolled metal, anisotropic friction in the clamping areas has to be considered [2]. On the other hand, recent studies show that intentional surface texturing can be beneficial to friction control in sheet metal forming [3]. In addition, anisotropic friction properties might be exploited for specific applications such as snake robots [4] and vibratory parts manipulation [5]. Many surfaces show orthotropic characteristics with different friction coefficients in different principal directions. In this work, orthotropic force laws are discussed, but the presented concept is valid for a broader range of anisotropic force laws. Friction measurements show that the magnitude of the friction force varies if a body is sliding along different directions. Furthermore, it can be observed that a body sliding on an anisotropic surface is deflected, indicating that the friction force is not acting collinear to the sliding direction. Therefore, for an accurate description of anisotropic friction, the set of admissible friction forces and the relation between the sliding direction and the direction of the friction force has to be specified.

The classical Coulomb friction law describes the constitutive behavior of stick and slip. In order to allow for a numerical treatment of the force law, it is often regularized. However, regularizations of the Coulomb friction law lack the ability to describe stiction, which motivates the use of set-valued force laws. This non-smooth approach makes use of methods of convex analysis such as normal cone inclusions. Normality of the sliding direction on the friction force reservoir corresponding to the principle of maximal dissipation is often assumed in the literature (see [6] and references therein). However, modeling anisotropic friction by a tribological microstructure with inclined planes leads to force laws in which normality to the force reservoir is no longer given and the force reservoir is not necessarily convex [7, 8]. A wide range of force laws can be described by using a convex force reservoir and a non-associated sliding rule [9].

In this work, various existing anisotropic dry friction models are formulated in the normal cone inclusion framework. We propose a force law within convex analysis based on the model developed in [7–9]. Our work thereby extends the model of [9], which is limited to ellipsoidal force reservoirs, to non-convex star-shaped force reservoirs. The normal cone inclusion force laws are implemented for numerical treatment using a Moreau time-stepping method [10] and numerical results are presented.

2 Normal cone inclusion force laws

In order to formulate set-valued force laws, concepts of convex analysis are used. In the following, a brief introduction in the topic is given. For more details the reader is referred to [6, 11]. A set $\mathscr{C} \subset \mathbb{R}^n$ is called convex if for each $\mathbf{x} \in \mathscr{C}$ and $\mathbf{y} \in \mathscr{C}$ also $(1-q)\mathbf{x}+q\mathbf{y} \in \mathscr{C}$ for all q with $0 \leq q \leq 1$. In this work, sets in $\mathbb{R}^2$ are discussed. Furthermore, a set $\mathscr{K} \subset \mathbb{R}^n$ is called a cone if $p\mathbf{x} \in \mathscr{K}$ for all $\mathbf{x} \in \mathscr{K}$ for all $p > 0$. A cone of special importance is the normal cone $\mathscr{N}_{\mathscr{C}}$ to a closed convex set $\mathscr{C}$ which is defined by

$$\mathscr{N}_{\mathscr{C}}(\mathbf{x}) = \left\{ \mathbf{y} \mid \mathbf{y}^{\mathrm{T}}(\mathbf{x}^* - \mathbf{x}) \leq 0, \mathbf{x} \in \mathscr{C}, \forall \mathbf{x}^* \in \mathscr{C} \right\}. \tag{1}$$

If a point $\mathbf{x}$ is in the interior of $\mathscr{C}$, then $\mathscr{N}_{\mathscr{C}}(\mathbf{x}) = \mathbf{0}$ and in the case $\mathbf{x} \notin \mathscr{C}$ the normal cone is the empty set. If $\mathbf{x}$ is on the boundary of $\mathscr{C}$, then the normal cone returns the set of all normal vectors to $\mathscr{C}$ at $\mathbf{x}$.

In the following, two rigid bodies that are in contact are considered. The two-dimensional vector of the relative sliding velocity at the contact point is denoted as $\boldsymbol{\gamma}_T = \begin{bmatrix} \gamma_{T_1} & \gamma_{T_2} \end{bmatrix}^{\mathrm{T}}$, the friction force as $\boldsymbol{\lambda}_T = \begin{bmatrix} \lambda_{T_1} & \lambda_{T_2} \end{bmatrix}^{\mathrm{T}}$ and the scalar normal force as λ_N. The spatial isotropic Coulomb friction law can be written as

$$\begin{array}{lll} \text{- stick} & \boldsymbol{\gamma}_T = \mathbf{0}\,; & \|\boldsymbol{\lambda}_T\| \leq \mu\lambda_N, \\ \text{- slip} & \boldsymbol{\gamma}_T \neq \mathbf{0}\,; & -\boldsymbol{\lambda}_T = \mu\lambda_N \frac{\boldsymbol{\gamma}_T}{\|\boldsymbol{\gamma}_T\|}, \end{array}$$

with μ being the friction coefficient. Rewriting the constitutive behavior of stick and slip as a normal cone inclusion yields

$$\boldsymbol{\gamma}_T \in \mathscr{N}_{\mathscr{C}}(-\boldsymbol{\lambda}_T). \tag{2}$$

The set $\mathscr{C}$, containing all admissible friction forces, is called force reservoir. In the isotropic case, it is the disc $\mathscr{C} = \left\{ -\boldsymbol{\lambda}_T \in \mathbb{R}^2 \mid \|\boldsymbol{\lambda}_T\| \leq \mu\lambda_N \right\}$. The inclusion (2) describes the set-valued force law of spatial isotropic friction. It accurately accounts for stiction, since if $-\boldsymbol{\lambda}_T \in \operatorname{int}\mathscr{C}$ it follows that $\mathscr{N}_{\mathscr{C}}(-\boldsymbol{\lambda}_T) = \mathbf{0}$.

Based on two assumptions, the normal cone inclusion force law for isotropic Coulomb friction is readily extended to anisotropic friction. First, the shape of the force reservoir has to be adjusted. For orthotropic friction, often an elliptical force reservoir of the form

$$\mathscr{C} = \left\{ -\boldsymbol{\lambda}_T \in \mathbb{R}^2 \;\middle|\; \sqrt{\left(\frac{\lambda_{T_1}}{\mu_1}\right)^2 + \left(\frac{\lambda_{T_2}}{\mu_2}\right)^2} \leq \lambda_N \right\} \tag{3}$$

is assumed, where μ_1 and μ_2 represent the friction coefficients along the two principal axes. In addition to the magnitude of the sliding force, which is defined by the shape of the force reservoir, the relation between the sliding direction and the direction of the friction force needs to be defined. If the principle of maximal dissipation is assumed to hold, then the vector $-\boldsymbol{\lambda}_T \in \mathscr{C}$ always maximizes the dissipation $D(\boldsymbol{\gamma}_T) = -\boldsymbol{\lambda}_T^{\mathrm{T}}\boldsymbol{\gamma}_T$ for a given $\boldsymbol{\gamma}_T$ [6]. Thus,

$$-\boldsymbol{\lambda}_T^{\mathrm{T}}\boldsymbol{\gamma}_T \geq -\boldsymbol{\lambda}_T^{*\mathrm{T}}\boldsymbol{\gamma}_T \quad \forall\, -\boldsymbol{\lambda}_T^* \in \mathscr{C}; \quad -\boldsymbol{\lambda}_T \in \mathscr{C}. \tag{4}$$

Comparing this inequality with the definition of a normal cone (1) reveals that the force law can again be written in the form of inclusion (2). Therefore, spatial anisotropic friction under the assumption of maximal dissipation is represented by the same inclusion as isotropic friction by adjusting the force reservoir $\mathscr{C}$. Figure 1(a) depicts a body sliding over an anisotropic surface with the sliding velocity $\boldsymbol{\gamma}_T$. The surface shows an orthotropic frictional behavior with the friction coefficients μ_1 and μ_2 along two orthogonal directions. The elliptical force reservoir

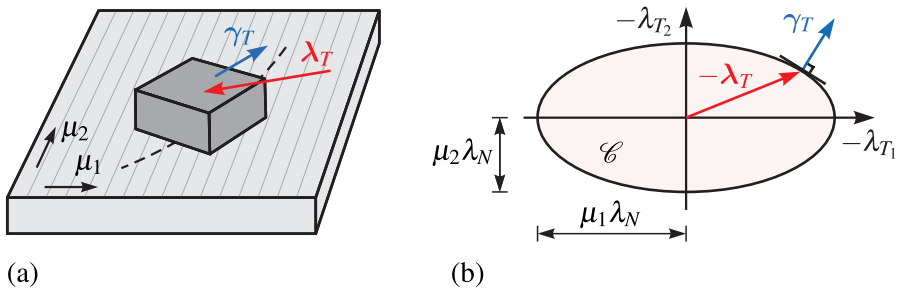

(a) (b)

Fig. 1: (a) Body sliding over anisotropic surface. (b) Normal cone inclusion force law with elliptical force reservoir.

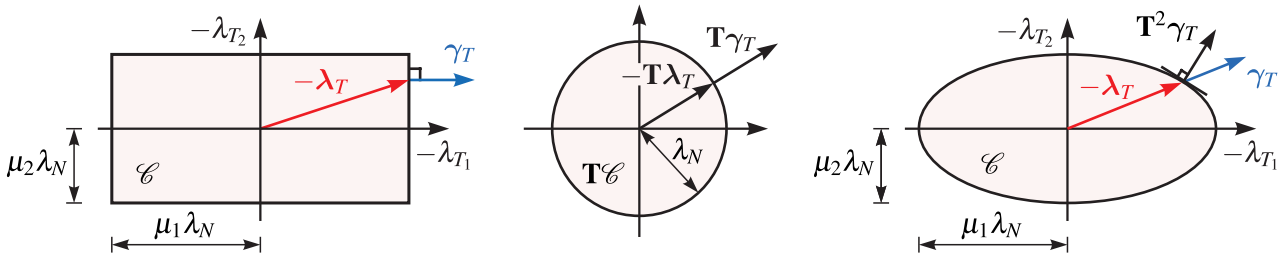

(a) (b) (c)

Fig. 2: (a) Normal cone inclusion force law on rectangular force reservoir. (b) Collinear force law transformed to circle. (c) Collinear force law with elliptical force reservoir

and the relationship between the sliding direction and the friction force according to inclusion (2) are shown in Fig. 1(b). In the case of a noncircular force reservoir, the sliding direction and the friction force are not collinear which causes the sliding body to deflect. The elliptical force reservoir and the principle of maximal dissipation are assumptions and therefore not necessarily valid for real anisotropic frictional behavior. In the following, two other friction models are briefly discussed and the force laws are rewritten as normal cone inclusions allowing for a numerical treatment as described in Section 4.

A different approach of introducing anisotropy in spatial Coulomb friction is the use of two sign functions [12]. To account for the set-valued nature of Coulomb friction we rewrite the force law using set-valued Sign functions leading to the inclusions

$$\begin{aligned} -\lambda_{T_1} &\in -\lambda_N \mu_1 \mathrm{Sign}(\gamma_{T_1}), \\ -\lambda_{T_2} &\in -\lambda_N \mu_2 \mathrm{Sign}(\gamma_{T_2}). \end{aligned} \tag{5}$$

Here, stick and slip along the two semi-axes are independent of each other. The inclusions (5) are equivalent to the normal cone inclusion (2) with a rectangular force reservoir $\mathscr{C}$. This case is shown in Fig. 2(a). The force reservoir is convex, but no longer strictly convex. A third type of anisotropic friction law is the collinear law [2] which can be expressed in the form

$$\gamma_T \neq 0\,; \quad -\boldsymbol{\lambda}_T = \mu(\gamma_T)\lambda_N \frac{\gamma_T}{\|\gamma_T\|}. \tag{6}$$

In this case, the friction force always directly opposes the sliding direction. Only the magnitude of the friction force varies because of the dependence of μ on the sliding direction. The force reservoir is assumed to be an ellipse. We convert the force law into a normal cone inclusion by making use of the transformation property for a linear mapping $\mathbf{A}$ derived in [13]

$$\mathbf{y} \in \mathscr{N}_{\mathscr{C}}(\mathbf{x}) \iff \mathbf{A}^{\mathrm{T}}\mathbf{y} \in \mathscr{N}_{\mathbf{A}^{-1}\mathscr{C}}(\mathbf{A}^{-1}\mathbf{x}). \tag{7}$$

The transformed set $\mathbf{A}^{-1}\mathscr{C}$ is thereby defined by containing every vector $\mathbf{A}^{-1}\mathbf{x}$ with $\mathbf{x} \in \mathscr{C}$. Considering the fact, that under the linear mapping $\mathbf{T}$ with

$$\mathbf{T} = \begin{bmatrix} \frac{1}{\mu_1} & 0 \\ 0 & \frac{1}{\mu_2} \end{bmatrix} \tag{8}$$

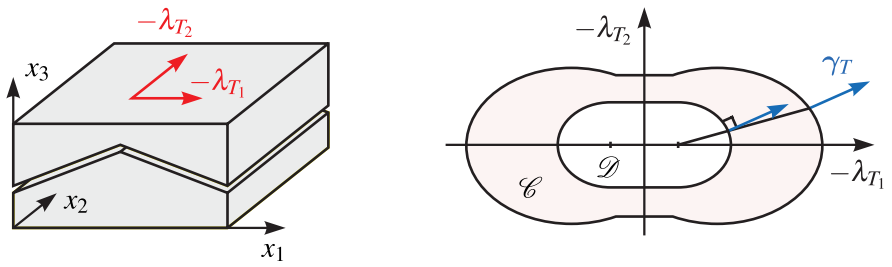

Fig. 3: (a) Model with symmetric wedge asperity. (b) Resulting non-convex force reservoir, modified from [7].

the collinear vectors $-\boldsymbol{\lambda}_T$ and $\boldsymbol{\gamma}_T$ remain collinear, the force law can be described by the graph shown in Fig. 2(b). The transformation matrix $\mathbf{T}$ is chosen such that the elliptical set $\mathscr{C}$ is transformed to the circular set $\mathbf{T}\mathscr{C}$. It is obvious that the law is represented by the inclusion

$$\mathbf{T}\boldsymbol{\gamma}_T \in \mathscr{N}_{\mathbf{T}\mathscr{C}}(-\mathbf{T}\boldsymbol{\lambda}_T). \tag{9}$$

This inclusion can be transformed to a normal cone inclusion on the force reservoir $\mathscr{C}$ using (7) with $\mathbf{A} = \mathbf{T}$ to

$$\mathbf{T}^2\boldsymbol{\gamma}_T \in \mathscr{N}_{\mathscr{C}}(-\boldsymbol{\lambda}_T). \tag{10}$$

Figure 2(c) shows the graph of this force law. A whole class of further anisotropic dry friction force laws is presented in the next section.

3 Asperity model

In [7] sliding rules are compared to plastic flow rules for perfectly plastic materials. It is stated that normality rules following from the principle of maximal dissipation are not valid in general. Using a model where the frictional anisotropy is imposed through unidirectional wedge asperities, it is found that in addition to the friction force reservoir $\mathscr{C}$ a second set $\mathscr{D}$ can be specified which is used to define the sliding direction by normality. In general, the friction force reservoir $\mathscr{C}$ is of different shape than the set $\mathscr{D}$. Therefore, the direction of the sliding velocity is not normal to $\mathscr{C}$.

If sliding on an anisotropic surface is modeled by sliding on an inclined plane having isotropic friction properties, both $\mathscr{C}$ and $\mathscr{D}$ are ellipses but with different semi-axes ratios and centered around different points. Figure 3(a) shows a wedge asperity with the same inclination angle on each side. This model leads to the non-convex force reservoir and the convex set $\mathscr{D}$ depicted in Fig. 3(b). In [8] the asperity model is extended by using one orthotropic surface with parallel wedge asperities and the opposing surface with isotropically distributed spring asperities. The set $\mathscr{D}$ remains of elliptical shape whereas $\mathscr{C}$ now varies between an ellipse and a non-convex shape similar to the one shown in Fig. 3(b) for different values of μ and the inclination angle of the wedge asperities. In the literature, the non-convex force reservoir is approximated by an ellipse. The force law then consists of the two ellipses $\mathscr{C}$ and $\mathscr{D}$ with different semi-axis ratios (see Fig. 4). Hjiaj et al. [9] further generalize the so-called non-associated force law by allowing for superelliptical shapes for $\mathscr{C}$ and $\mathscr{D}$. This leads to a very general force law enabling to represent various physical mechanisms by adjusting the semi-axis ratios and roundness factors s of the superellipses. The shape of superellipses can be varied between a parallelogram and a rectangle. Only standard ellipses or superellipses with the same roundness factors for $\mathscr{C}$ and $\mathscr{D}$ have been used in numerical simulations [9].

To analyze the existence of a convex pseudo-potential, the force law has to be checked for cyclic maximal monotonicity [11]. It is seen that for different shapes of $\mathscr{C}$ and $\mathscr{D}$ two pairs of $\boldsymbol{\lambda}_T$ and $\boldsymbol{\gamma}_T$ can be chosen such that

$$(-\boldsymbol{\lambda}_{T_I} - (-\boldsymbol{\lambda}_{T_{II}}))^{\mathrm{T}}(\boldsymbol{\gamma}_{T_I} - \boldsymbol{\gamma}_{T_{II}}) < 0. \tag{11}$$

Thus, the monotonicity condition is not fulfilled and since cyclic maximal monotonicity is a stronger condition than monotonicity, a convex pseudo-potential does not exist. Instead, following [9], a bipotential can be found. For

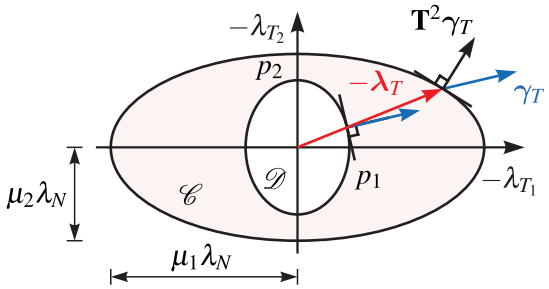

Fig. 4: Force law with elliptical force reservoir and normality to elliptical set $\mathscr{D}$.

a known normal force the bipotential for the case of superelliptical $\mathscr{C}$ and $\mathscr{D}$ with roundness factor s, is given as

$$b_{\mathscr{C}}(\boldsymbol{\gamma}_T, -\boldsymbol{\lambda}_T) = \Psi_{\mathscr{C}}(-\boldsymbol{\lambda}_T) + (\mathbf{I} - \mathbf{T}^s)(-\boldsymbol{\lambda}_T)\boldsymbol{\gamma}_T + \Psi^*_{\mathscr{C}}(\mathbf{T}^s\boldsymbol{\gamma}_T), \tag{12}$$

where $\mathbf{T}$ is defined by the semi-axis ratios as

$$\mathbf{T} = \begin{bmatrix} \frac{p_1}{\mu_1} & 0 \\ 0 & \frac{p_2}{\mu_2} \end{bmatrix}. \tag{13}$$

The indicator function $\Psi_{\mathscr{C}}(-\boldsymbol{\lambda}_T)$ is 0 if $-\boldsymbol{\lambda}_T \in \mathscr{C}$ and $+\infty$ otherwise. The bipotential is convex with respect to $\boldsymbol{\gamma}_T$ for fixed $\boldsymbol{\lambda}_T$ and vice versa. Taking the subdifferential of the bipotential as

$$\boldsymbol{\gamma}_T \in \partial_{-\boldsymbol{\lambda}_T} b_{\mathscr{C}}(\boldsymbol{\gamma}_T, -\boldsymbol{\lambda}_T) \tag{14}$$

and recalling that the subdifferential of an indicator function equals the normal cone, the normal cone inclusion force law

$$\mathbf{T}^s\boldsymbol{\gamma}_T \in \mathscr{N}_{\mathscr{C}}(-\boldsymbol{\lambda}_T) \tag{15}$$

is obtained. This inclusion is similar to (10). Indeed, the collinear force law presented in Section 2 is equivalent to the force law described here when a circular set $\mathscr{D}$ is used. Obviously, if $\mathscr{D}$ is chosen equal to $\mathscr{C}$, the standard normal cone inclusion force law for anisotropic friction is obtained. The inclusion (15) is a useful description of an anisotropic friction force law for superelliptical shapes of $\mathscr{C}$ and $\mathscr{D}$ with identical roundness factors. In this work, the model described by (15) is extended to allow for superellipses having different roundness factors and non-convex force reservoirs. In order to generalize the law, gauge functions can be utilized. The gauge function $k_{\mathscr{C}}$ of the set $\mathscr{C}$ is a nonnegative, positively homogeneous (of degree one) function [14] defined by

$$k_{\mathscr{C}}(\mathbf{x}) = \inf\{q > 0 \mid \mathbf{x} \in q\mathscr{C}\}. \tag{16}$$

Level sets of gauge functions are therefore given as

$$\mathscr{C} = \{-\boldsymbol{\lambda}_T \mid k_{\mathscr{C}}(-\boldsymbol{\lambda}_T) \leq 1\}, \quad \mathscr{D} = \{-\boldsymbol{\lambda}_T \mid k_{\mathscr{D}}(-\boldsymbol{\lambda}_T) \leq 1\}. \tag{17}$$

One approach to extend (15) is to change the left-hand side of (15) and to still have a normal cone inclusion on the force reservoir $\mathscr{C}$. The advantage is, that the condition $\boldsymbol{\gamma}_T = \mathbf{0}$ for friction forces inside the force reservoir is automatically fulfilled. However, since the normal cone inclusion is only defined for convex sets, the force reservoir is limited to convex shapes. In this work, we propose to formulate the law as normal cone inclusion on $\mathscr{D}$. Here, the normality condition is directly fulfilled and non-convex force reservoirs are no longer excluded. The challenge is the accurate description of stick since the force reservoir is independent of $\mathscr{D}$. The complete force law can be formulated as

$$\begin{cases} \boldsymbol{\gamma}_T \in \mathscr{N}_{\mathscr{D}}(-\alpha\boldsymbol{\lambda}_T) & \text{for} \quad -\boldsymbol{\lambda}_T \in \operatorname{bdry}\mathscr{C} \quad \text{with} \quad -\alpha\boldsymbol{\lambda}_T \in \operatorname{bdry}\mathscr{D} \\ \boldsymbol{\gamma}_T = \mathbf{0} & \text{for} \quad -\boldsymbol{\lambda}_T \in \operatorname{int}\mathscr{C}. \end{cases} \tag{18}$$

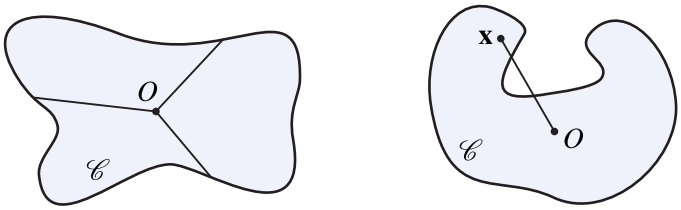

(a) (b)

Fig. 5: (a) Star-shaped set. (b) Not star-shaped set.

It can be rewritten by making use of the gauge functions $k_{\mathscr{C}}$ and $k_{\mathscr{D}}$,

$$\begin{cases} \boldsymbol{\gamma}_T \in \mathscr{N}_{\mathscr{D}}(-\alpha\boldsymbol{\lambda}_T) & \text{for} \quad k_{\mathscr{C}}(-\boldsymbol{\lambda}_T) = 1 \quad \text{with} \quad k_{\mathscr{D}}(-\alpha\boldsymbol{\lambda}_T) = 1 \\ \boldsymbol{\gamma}_T = \mathbf{0} & \text{for} \quad k_{\mathscr{C}}(-\boldsymbol{\lambda}_T) < 1. \end{cases} \tag{19}$$

To write (19) as one normal cone inclusion, we design the scaling function $\alpha = f(-\boldsymbol{\lambda}_T)$ as

$$\alpha : \begin{cases} = \frac{1}{k_{\mathscr{D}}(-\boldsymbol{\lambda}_T)} & \text{for} \quad -\boldsymbol{\lambda}_T \in \operatorname{bdry}\mathscr{C} \\ < \frac{1}{k_{\mathscr{D}}(-\boldsymbol{\lambda}_T)} & \text{for} \quad -\boldsymbol{\lambda}_T \in \operatorname{int}\mathscr{C}. \end{cases} \tag{20}$$

The following function combines these conditions

$$\alpha = \frac{1}{k_{\mathscr{D}}(-\boldsymbol{\lambda}_T) - k_{\mathscr{C}}(-\boldsymbol{\lambda}_T) + 1}. \tag{21}$$

Finally, (19) can be written in a compact form as

$$\boldsymbol{\gamma}_T \in \mathscr{N}_{\mathscr{D}}(-\alpha\boldsymbol{\lambda}_T). \tag{22}$$

The scaling function α is defined for all nonempty sets $\mathscr{D}$ and $-\boldsymbol{\lambda}_T \in \mathscr{C}$. The normal cone inclusion force law is numerically evaluated using proximal point functions as described in the following section. The argument thereby possibly exceeds the limits of the set $\mathscr{C}$. To ensure that the scaling function α is always defined, we impose the condition $k_{\mathscr{D}}(-\boldsymbol{\lambda}_T) \geq k_{\mathscr{C}}(-\boldsymbol{\lambda}_T)$. Therefore, $\mathscr{D} \subset \mathscr{C}$ must apply. This can be reached for all $\mathscr{C}$ with $\operatorname{int}\mathscr{C} \neq \emptyset$ since the set $\mathscr{D}$ can always be scaled without loss of generality. The advantage of this approach is that the force reservoir is no longer restricted to convex shapes. The definitions of gauge functions Eq. (16) and corresponding level sets Eq. (17) are also valid for sets that are star-shaped with respect to the origin [14]. Therefore, for all closed sets $\mathscr{C} \subset \mathbb{R}^n$ that fulfill the condition,

$$\text{if} \quad \mathbf{x} \in \mathscr{C} \quad \text{then} \quad \alpha\mathbf{x} \in \mathscr{C} \quad \forall\, \alpha \in [0,1]\,. \tag{23}$$

These star-shaped sets are possibly non-convex. Figure 5 shows an example of a non-convex star-shaped set and of a set which is not star-shaped. Limiting the force reservoir $\mathscr{C}$ to star-shaped and the set $\mathscr{D}$ to convex shapes ensures that for a given $\boldsymbol{\gamma}_T$ a unique friction force $\boldsymbol{\lambda}_T$ is assigned. All the force laws given as normal cone inclusions can be used for numerical simulations as shown in the following section.

4 Numerical simulation

In the following, the numerical simulation procedure is briefly discussed before numerical examples are given. As described above, anisotropic friction force laws are formulated as normal cone inclusions either on $\mathscr{C}$ or $\mathscr{D}$. These inclusions can be rewritten as implicit equations using proximal point functions [6] according to

$$\boldsymbol{\gamma}_T \in \mathscr{N}_{\mathscr{C}}(-\boldsymbol{\lambda}_T) \Longleftrightarrow -\boldsymbol{\lambda}_T = \operatorname{prox}_{\mathscr{C}}(-\boldsymbol{\lambda}_T + r\boldsymbol{\gamma}_T), \quad r > 0, \tag{24}$$

$$\boldsymbol{\gamma}_T \in \mathscr{N}_{\mathscr{D}}(-\alpha\boldsymbol{\lambda}_T) \Longleftrightarrow -\alpha\boldsymbol{\lambda}_T = \operatorname{prox}_{\mathscr{D}}(-\alpha\boldsymbol{\lambda}_T + r\boldsymbol{\gamma}_T), \quad r > 0. \tag{25}$$

The proximal point function of a point $\mathbf{z}$ to a convex set $\mathscr{D}$ returns the closest point $\mathbf{x}$ of the set $\mathscr{D}$ to $\mathbf{z}$. In the following, two possibilities to calculate the proximal point function on an ellipse are described [15]. For the projection method, it first has to be checked whether $\mathbf{z} \in \mathscr{D}$ which implies $\mathbf{x} = \mathbf{z}$. If not, the proximal point is calculated using the following conditions,

$$\mathbf{x} = \text{prox}_{\mathscr{D}}(\mathbf{z}) \Longrightarrow \mathbf{x} + \beta \nabla k_{\mathscr{D}}(\mathbf{x}) = \mathbf{z}, \quad k_{\mathscr{D}}(\mathbf{x}) = 1. \tag{26}$$

To determine β, a fourth order polynomial has to be solved. The proximal point is computed by using the positive real solution for β. The second method is based on the transformation of the normal cone on an ellipse to the normal cone on a circle according to relationship (7). Then, the proximal point of a circular set needs to be calculated.

The equation of motion of a multibody system with closed contacts is given as

$$\mathbf{M}(t,\mathbf{q})\dot{\mathbf{u}} - \mathbf{h}(t,\mathbf{q},\mathbf{u}) = \mathbf{W}_T \boldsymbol{\lambda}_T, \tag{27}$$

where $\mathbf{M}$ is the mass matrix, $\mathbf{q}$ the vector of generalized coordinates and $\mathbf{u}$ the vector of generalized velocities. The vector $\mathbf{h}$ contains all forces besides the contact forces and $\mathbf{W}_T$ is the matrix of generalized force directions. The equation of motion can be replaced by the equality of measures [10]

$$\mathbf{M}(t,\mathbf{q})\mathrm{d}\mathbf{u} - \mathbf{h}(t,\mathbf{q},\mathbf{u})\mathrm{d}t = \mathbf{W}_T \mathrm{d}\mathbf{P}_T. \tag{28}$$

The vector $\mathrm{d}\mathbf{P}_T$ denotes the contact effort measure. In Moreau's time-stepping scheme, the equality of measures is approximated over small time-steps Δt. The subscripts A, M and E are used to describe values at the beginning, midpoint and end of a time-step, respectively. The values at the beginning are known and the values at the midpoint are calculated using the midpoint rule. If the force law is formulated as normal cone inclusion on $\mathscr{D}$, for each time step the inclusion problem

$$\begin{aligned} &\mathbf{M}_M(\mathbf{u}_E - \mathbf{u}_A) - \mathbf{h}_M \Delta t = \mathbf{W}_{TM}\mathbf{P}_T, \\ &\boldsymbol{\gamma}_{TE} \in \mathscr{N}_{\mathscr{D}}(-\alpha \mathbf{P}_T), \quad \alpha = \frac{1}{k_{\mathscr{D}}(-\mathbf{P}_T) - k_{\mathscr{C}}(-\mathbf{P}_T) + 1} \end{aligned} \tag{29}$$

needs to be considered. Thereby, the contact problem is solved using an initial guess and iterating

$$\mathbf{P}_T^{k+1} = -\frac{1}{\alpha^k}\text{prox}_{\mathscr{D}}(-\alpha^k \mathbf{P}_T^k + r\boldsymbol{\gamma}^k{}_{TE}), \quad r > 0 \tag{30}$$

until a stopping criterion is reached.

4.1 Force laws with ellipsoidal sets

The described time-stepping scheme can be used to compare different force laws. As an example, a body with initial velocity $\mathbf{u}_0$ sliding on a horizontal orthotropic surface is considered. Its coordinates are q_1 and q_2. The contact is always closed and the normal force λ_N resulting from the weight of the body is constant. The friction coefficients along the principal axes of the orthotropic surface are μ_1 and μ_2 with $\mu_1 > \mu_2$ and the shape of the force reservoir is elliptic. The sets $\mathscr{D}$ are also ellipses with the same principal directions as $\mathscr{C}$. The semi-axis ratio p_1/p_2 is varied (see Fig. 6(a)). The sliding paths of the body until stick are calculated using inclusion (22) for each set $\mathscr{D}$ and plotted in Fig. 6(b). For a circular set $\mathscr{D}$ the friction force always directly opposes the sliding direction, which leads to a linear sliding path (green). In all other cases, the sliding body is deflected. A larger ratio p_1/p_2 thereby causes a larger deflection towards the direction of lower friction coefficient. The case $p_1/p_2 = \mu_1/\mu_2$ is shown in blue. It corresponds to the normal cone inclusion force law based on the principle of maximal dissipation (2). For $p_1 < p_2$ contrary to intuition, the body is deflected in the direction of the higher friction coefficient.

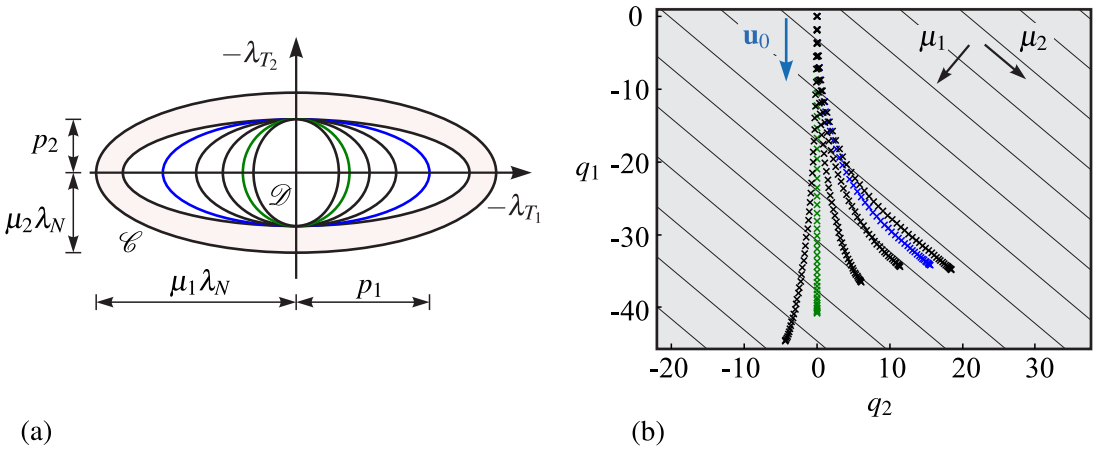

Fig. 6: (a) Elliptical force reservoir and different elliptical sets $\mathscr{D}$. (b) Sliding paths for different sets $\mathscr{D}$.

4.2 Non-convex friction force reservoir

The advantage of the force law formulated as normal cone inclusion on $\mathscr{D}$ is, that the sets $\mathscr{C}$ and $\mathscr{D}$ can be of different shape and even non-convex friction force reservoirs $\mathscr{C}$ are possible. This example demonstrates the ability of the simulation procedure to handle non-convex force reservoirs. The force reservoir is arbitrarily chosen as level set of the gauge function

$$k_{\mathscr{C}}(-\boldsymbol{\lambda}_T) = \frac{5}{2}\left(\left[\left(\frac{\lambda_{T_1}}{\mu_1\lambda_N}\right)^2 + \left(\frac{\lambda_{T_2}}{\mu_2\lambda_N}\right)^2\right]^{\frac{1}{2}} - \frac{3}{5}\left[\left(\frac{\lambda_{T_1}}{\mu_1\lambda_N}\right)^4 + \left(\frac{\lambda_{T_2}}{\mu_2\lambda_N}\right)^4\right]^{\frac{1}{4}}\right), \tag{31}$$

whereas $\mathscr{D}$ is an ellipse with semi-axes p_1 and p_2. The gauge function $k_{\mathscr{C}}$ is the sum of a 2- and 4-norm scaled such that the semi-axes are $\mu_1\lambda_N$ and $\mu_2\lambda_N$. It holds that $p_1/p_2 = \mu_1/\mu_2$. In the simulation, a body is sliding along a prescribed circle on a surface having othotropic friction properties. The angular velocity is constant. According to the normal cone inclusion on $\mathscr{D}$ (22) the friction force is calculated implicitly at each time step. The calculated friction forces are shown in Fig. 7 (red). In addition, the chosen set $\mathscr{D}$ and the sliding velocities at each time step are plotted in the figure. The calculated friction forces are laying on the boundary of the chosen friction force reservoir and demonstrate its non-convex shape. The vectors of the sliding velocity are not normal to the force reservoir, but to the set $\mathscr{D}$.

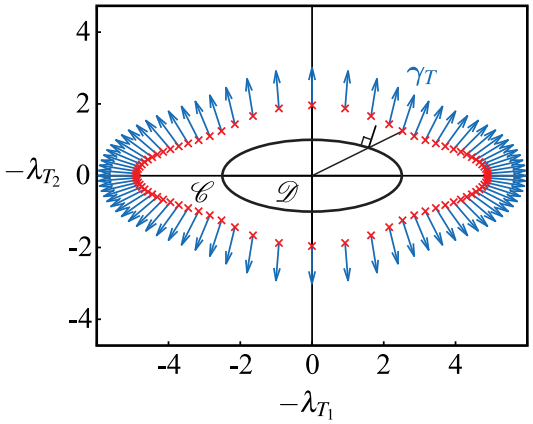

Fig. 7: Force law with generic non-convex force reservoir.

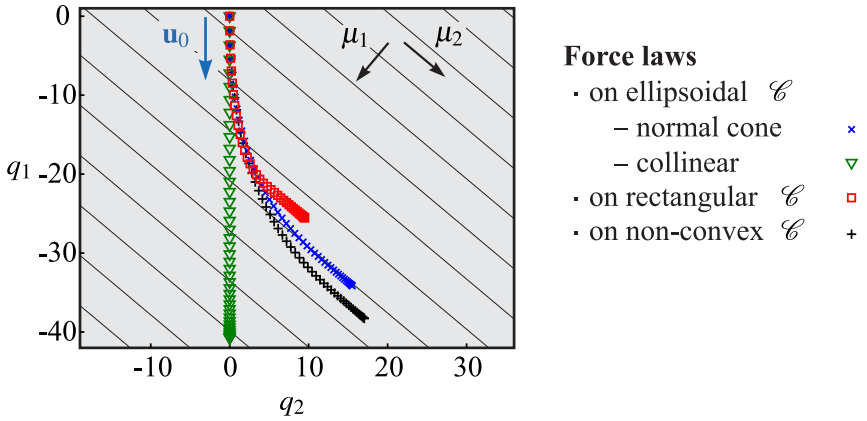

Fig. 8: Sliding paths for different force laws.

4.3 Force laws with various force reservoirs

Again, a body sliding on an orthotropic surface as described in Section 4.1 is considered. Four of the force laws described above are implemented. The normal cone inclusion force law (2) is used in combination with an ellipsoidal and a rectangular force reservoir $\mathscr{C}$. The collinear force law (10) is applied on an ellipsoidal force reservoir and the normal cone inclusion on $\mathscr{D}$ (22) is utilized with the non-convex friction force reservoir defined by the level set of the gauge function (31). In all cases, the friction coefficients along the semi-axes μ_1 and μ_2 are the same, respectively. Figure 8 shows the numerical results of the sliding paths for the force laws until stick. Naturally, the collinear force law leads to a linear sliding path. The results of the sliding paths using the collinear force law and the force law based on the principle of maximal dissipation formulated as normal cone inclusion on $\mathscr{C}$ are equivalent to the results obtained using the formulation as normal cone inclusion on $\mathscr{D}$ in Section 4.1. The rectangular force reservoir leads to a large deflection of the body and allows for large friction forces, causing the body to stick after a shorter sliding path. In contrast, the admissible friction forces in the case of the chosen non-convex force reservoir are the lowest.

5 Conclusions

Finding an accurate description of anisotropic dry friction is a challenging task. In this work, it is shown that various force laws can be cast in the normal cone inclusion framework. Normal cone inclusions are a useful tool to describe the set-valued nature of Coulomb dry friction. By using gauge functions, existing force laws are extended to allow for non-convex force reservoirs. The proposed normal cone inclusion force law is implemented in a Moreau time-stepping scheme and numerical results are given. The results demonstrate the capability of the force law to handle non-convex star-shaped force reservoirs. Furthermore, the results show that despite using the same friction coefficients along the principal axes of an orthotropic surface, the frictional behavior heavily depends on the shape of the friction force reservoir and the convex set $\mathscr{D}$. We conclude that in order to accurately predict the behavior of real systems, great care has to be taken in the modeling of anisotropic friction. In future work, the highly general force law with star-shaped force reservoir and independent set $\mathscr{D}$ can be used to describe measured anisotropic frictional behavior.

References

[1] A. Zmitrowicz, “Models of kinematics dependent anisotropic and heterogeneous friction,” *International Journal of Solids and Structures*, vol. 43, no. 14, pp. 4407–4451, 2006.

[2] M. Liewald, S. Wagner, and D. Becker, "New approaches on Coulomb's friction model for anisotropic sheet metal forming applications," in *Proceedings of the 9th ESAFORM Conference on Material Forming, Glasgow*, 2006.

[3] D. A. Aktürk, P. Liu, J. Cao, Q. J. Wang, Z. C. Xia, R. Talwar, D. Grzina, and M. Merklein, "Friction anisotropy of Aluminum 6111-T4 sheet with flat and laser-textured D2 tooling," *Tribology International*, vol. 81, pp. 333–340, 2015.

[4] A. A. Transeth, R. I. Leine, C. Glocker, and K. Y. Pettersen, "3-D snake robot motion: Nonsmooth modeling, simulations, and experiments," *IEEE Transactions on Robotics*, vol. 24, no. 2, pp. 361–376, 2008.

[5] P. Umbanhowar, T. H. Vose, A. Mitani, S. Hirai, and K. M. Lynch, "The effect of anisotropic friction on vibratory velocity fields," in *Proceedings of 2012 IEEE International Conference on Robotics and Automation*, pp. 2584–2591, 2012.

[6] R. I. Leine and N. van de Wouw, *Stability and Convergence of Mechanical Systems with Unilateral Constraints*, vol. 36 of *Lecture Notes in Applied and Computational Mechanics*. Berlin: Springer, 2008.

[7] R. Michalowski and Z. Mróz, "Associated and non-associated sliding rules in contact friction problems," *Archiv. Mech.*, vol. 30, pp. 259–276, 1978.

[8] Z. Mróz and S. Stupkiewicz, "An anisotropic friction and wear model," *International Journal of Solids and Structures*, vol. 31, no. 8, pp. 1113–1131, 1994.

[9] M. Hjiaj, Z.-Q. Feng, G. de Saxcé, and Z. Mróz, "On the modelling of complex anisotropic frictional contact laws," *International Journal of Engineering Science*, vol. 42, no. 10, pp. 1013–1034, 2004.

[10] J. J. Moreau, "Unilateral contact and dry friction in finite freedom dynamics," in *Nonsmooth Mechanics and Applications* (J. J. Moreau and P. D. Panagiotopoulos, eds.), pp. 1–82, Springer, Wien, 1988.

[11] R. T. Rockafellar and R. J.-B. Wets, *Variational Analysis*. Berlin: Springer, 1998.

[12] M. Saito, M. Fukaya, and T. Iwasaki, "Modeling, analysis, and synthesis of serpentine locomotion with a multilink robotic snake," *IEEE Control Systems Magazine*, vol. 22, no. 1, pp. 64–81, 2002.

[13] M. Möller, R. I. Leine, and C. Glocker, "An efficient approximation of orthotropic set-valued force laws of normal cone type," in *Proceedings of the 7th Euromech Solid Mechanics Conference, Lisbon*, pp. 7–11, 2009.

[14] V. F. Demyanov, G. E. Stavroulakis, L. N. Polyakova, and P. D. Panagiotopoulos, *Quasidifferentiability and Nonsmooth Modelling in Mechanics, Engineering and Economics*, vol. 10. Dordrecht: Springer Science & Business Media, 1996.

[15] C. Studer, *Numerics of Unilateral Contacts and Friction: Modeling and Numerical Time Integration in Non-Smooth Dynamics*, vol. 47 of *Lecture Notes in Applied and Computational Mechanics*. Berlin: Springer, 2009.